Detection of a Substantial Molecular Gas Reservoir in a Brightest Cluster Galaxy at $z = 1.7$

Tracy M. A. Webb[1], James Lowenthal[2], Min Yun[3], Allison G. Noble[4], Adam Muzzin[5], Gillian Wilson[6], H. K. C. Yee[7], Ryan Cybulski[3], I. Aretxaga[8], and D. H. Hughes[8]

[1] McGill Space Institute, Department of Physics, McGill University, 3600 rue University Montréal, Montréal, QC H3A 2T8, Canada; webb@physics.mcgill.ca
[2] Department of Astronomy, Smith College, Northampton, MA 01063, USA
[3] Department of Astronomy, University of Massachusetts, Amherst, MA 01003, USA
[4] Kavli Institute for Astrophysics and Space Research, Massachusetts Institute of Technology, 77 Massachusetts Avenue, Cambridge, MA 02139, USA
[5] Department of Physics and Astronomy, York University, 4700 Keele Street, Toronto, ON MJ3 1P3, Canada
[6] Department of Physics and Astronomy, University of California-Riverside, 900 University Avenue, Riverside, CA 92521, USA
[7] Department of Astronomy & Astrophysics, University of Toronto, 50 St. George Street, Toronto, ON M5S 3H4, Canada
[8] Instituto Nacional de Astrofisica, Optica y Electronica (INAOE), Aptdo. Postal 51 y 216, 72000 Puebla, Mexico
Received 2017 May 10; revised 2017 May 30; accepted 2017 May 30; published 2017 July 25

Abstract

We report the detection of CO(2–1) emission coincident with the brightest cluster galaxy (BCG) of the high-redshift galaxy cluster SpARCS1049+56, with the Redshift Search Receiver (RSR) on the Large Millimeter Telescope (LMT). We confirm a spectroscopic redshift for the gas of $z = 1.7091 \pm 0.0004$, which is consistent with the systemic redshift of the cluster galaxies of $z = 1.709$. The line is well fit by a single-component Gaussian with an RSR-resolution-corrected FWHM of $569 \pm 63 \, \mathrm{km \, s^{-1}}$. We see no evidence for multiple velocity components in the gas, as might be expected from the multiple image components seen in near-infrared imaging with the *Hubble Space Telescope*. We measure the integrated flux of the line to be $3.6 \pm 0.3 \, \mathrm{Jy \, km \, s^{-1}}$, and using $\alpha_{CO} = 0.8 \, M_\odot \, (\mathrm{K \, km \, s^{-1} \, pc^2})^{-1}$, we estimate a total molecular gas mass of $1.1 \pm 0.1 \times 10^{11} \, M_\odot$ and a $M_{H2}/M_\star \sim 0.4$. This is the largest gas reservoir detected in a BCG above $z > 1$ to date. Given the infrared-estimated star formation rate of $860 \pm 130 \, M_\odot \, \mathrm{yr^{-1}}$, this corresponds to a gas depletion timescale of ~ 0.1 Gyr. We discuss several possible mechanisms for depositing such a large gas reservoir to the cluster center—e.g., a cooling flow, a major galaxy–galaxy merger, or the stripping of gas from several galaxies—but conclude that these LMT data are not sufficient to differentiate between them.

Key words: galaxies: clusters: individual (SpARCS1049+56) – galaxies: evolution – galaxies: starburst – ISM: molecules

1. Introduction

Brightest cluster galaxies (BCGs) occupy special locations in the universe. Because of this they likely experience evolutionary paths that are likewise special and unique, compared to other massive galaxies. A picture has emerged where BCGs have grown in stellar mass by roughly a factor of 2 since $z \sim 1$ (e.g., Lidman et al. 2012; Zhang et al. 2016), through the dry accretion of satellite galaxies. In this scenario, most of the stellar mass of BCGs is produced at higher redshifts in smaller systems and assembled into the BCG at later times (De Lucia & Blaizot 2007). Evidence is now mounting, however, that beyond $z \sim 1$, significant in situ star formation may be occurring, rivaling the stellar mass build-up through dry mergers (Webb et al. 2015b; McDonald et al. 2016). Although the occurrence of star formation in high-redshift BCGs is now established, the processes that fuel and trigger the star formation are poorly understood.

At low redshifts, though rare, star-forming BCGs primarily reside in cool-core clusters and the star formation rate (SFR) is correlated with the cooling time of the X-ray gas (e.g., Rawle et al. 2012). This appears to indicate that star formation in low-redshift BCGs is fueled by large-scale cooling flows. Many of these systems also exhibit immense reservoirs of cold gas traced through the measurement of CO (e.g., Edge 2001). At higher redshifts, the situation is less clear, though McDonald et al. (2014) has detected CO(3–2) in the Phoenix cluster with similar morphology (Russell et al. 2016).

Recently, however, Webb et al. (2015b) and McDonald et al. (2016) have suggested that beyond $z \sim 1$ star formation in BCGs is driven by a different process: gas-rich major mergers occurring at the center of galaxy clusters. This conclusion is motivated by the change in slope of the specific SFR with redshift (McDonald et al. 2016) and one case study of an apparent gas-rich BCG merger (Webb et al. 2015a) in the galaxy cluster SpARCS1049+56.

SpARCS1049+56 is a $z = 1.7$ red-sequence-selected galaxy cluster with a star bursting core. This system is one of a larger sample of $0.3 < z < 1.8$ clusters, drawn from the Spitzer Adaptation of the Red Sequence Cluster Survey (SpARCS; Muzzin et al. 2009; Wilson et al. 2009), whose BCGs exhibit signs of intense star formation (Webb et al. 2015b; Bonaventura et al. 2017). It is spectroscopically confirmed through 27 cluster members (Webb et al. 2015a), and the richness-estimated mass of $M_{500 \, \mathrm{kpc}} \sim 4 \times 10^{14} \, M_\odot$ is in good agreement with the weak lensing estimate of $3 \times 10^{14} \, M_\odot$ (J. Jee 2017, personal communication). Its BCG is coincident with intense infrared emission of $L_{IR} = 6.2 \times 10^{12} \, L_\odot$ with an AGN-corrected SFR of $860 \, M_\odot \, \mathrm{yr^{-1}}$. The *Hubble Space Telescope* (*HST*) image has revealed optical morphology that is consistent with a major galaxy merger: a long tidal tail with >10 UV-luminous clumps arranged like "beads-on-a-string." These clumps appear to originate within the stellar halo of the BCG and extend for 60 kpc.

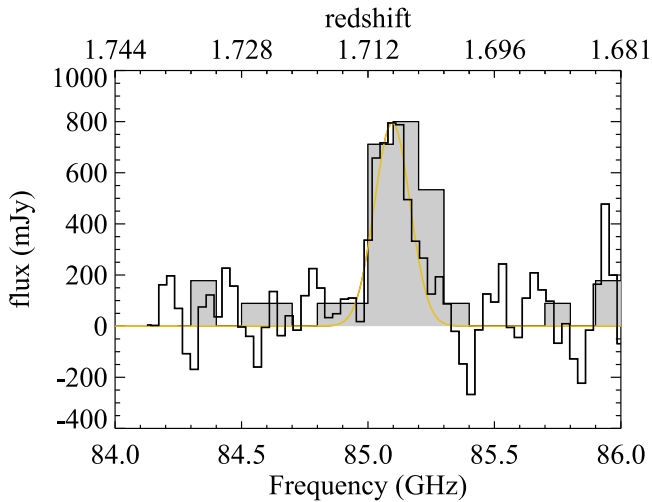Here, we present the detection of molecular gas in SpARCS1049+56 through a measurement of the CO (2–1)

Figure 1. Redshift Search Receiver spectrum showing the 10.7σ detection of CO (2–1), redshifted to $z = 1.7091$, as a solid black line. Overplotted (solid yellow line) is the best-fit Gaussian described in Section 3.1. Also shown are the locations in frequency space of the cluster galaxy members confirmed with optical spectroscopy (gray histogram).

line with the Redshift Search Receiver (RSR) on the Large Millimeter Telescope (LMT). To our knowledge, it is the first detection of molecular gas in a BCG beyond $z = 1$. It offers a new opportunity to study the gas that fuels star formation in BCGs at high redshift. In the following, we present the basic properties of the gas reservoir and discuss various gas deposition mechanisms.

Throughout, we choose a flat Λ cold dark matter cosmology with $H_\mathrm{o} = 75\ \mathrm{km\,s^{-1}\,Mpc^{-1}}$, $\Omega_\mathrm{m} = 0.3$, and $\Omega_\Lambda = 0.7$. When required, we adopt a Chabrier IMF.

2. Observations

2.1. Redshift Search Receiver Observations with the Large Millimeter Telescope

Observations were obtained using the RSR on the 32 meter LMT (Hughes et al. 2010) on 2016 April 11–12 and 2017 February 18–19 for a total of 6 hr. The wide bandwidth of the RSR covers the frequency window of 73–111 GHz simultaneously with a spectral resolution of 31.25 MHz ($110\ \mathrm{km\,s^{-1}}$ at 85 GHz). The redshifted CO (2–1) line ($\nu_0 = 230.5380$ GHz) at $z = 1.7$ falls near the center of the spectrometer band at $\nu_\mathrm{obs} \sim 85$ GHz. Observing conditions were excellent with $\tau_{225\,\mathrm{GHz}} = 0.05$–$0.15$. The final spectrum shown in Figure 1 was produced by calibrating and averaging the raw data using the facility data reduction software DREAMPY.

3. Results

3.1. Detection and Characterization of the CO Line

Figure 1 shows the RSR spectrum, zoomed in on the CO(2–1) line. To characterize the line, we performed MCMC fitting of a Gaussian function on the data (Cybulski et al. 2016). We fit over a 2 GHz bandwidth centered at 85 GHz, with a low-order baseline removal. We measure the integral line flux to be $3.59 \pm 0.34\ \mathrm{Jy\,km\,s^{-1}}$, providing detection significance of S/N = 10.7. The line centroid is 85.0961 ± 0.0131 GHz, and it has an RSR-resolution-corrected FWHM of $569 \pm 63\ \mathrm{km\,s^{-1}}$.
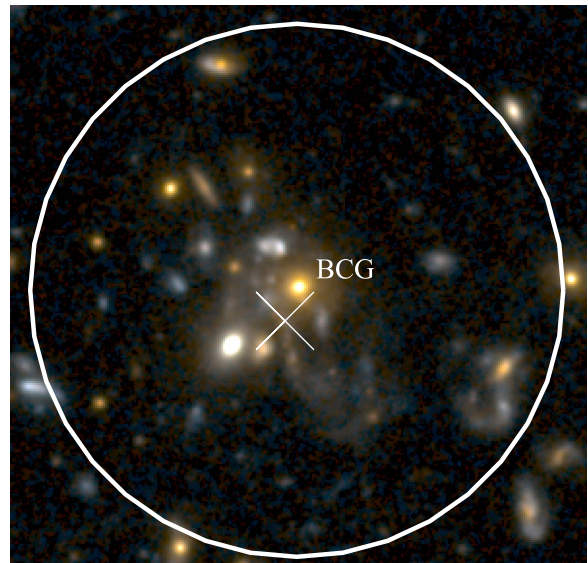

Figure 2. Three-color (F814W/F105W/F160W) *HST* image of the BCG and surrounding area. The large circle marks the size of the 25 arcsec FWHM beam of the LMT. The LMT was pointed at the BCG (the central bright yellow galaxy in the image) but the CO (2–1) emission may be coming from any galaxy within the beam, at $z = 1.709$. The location of the MIPS 24 μm centroid is shown by the white cross, with the size of the cross corresponding to the 1σ uncertainty in the MIPS position.

We calculate an integrated source brightness temperature of $1.16 \pm 0.10 \times 10^{11}\ \mathrm{K\,km\,s^{-1}\,pc^2}$ using

$$L'_\mathrm{CO} = 3.25 \times 10^7 \times S_\mathrm{CO}\Delta v \frac{D_L^2}{(1+z)^3 \nu_\mathrm{obs}^2}\ \mathrm{K\,km\,s^{-1}\,pc^2},\quad (1)$$

where $S_\mathrm{CO}\Delta v$ is the integral line flux in $\mathrm{Jy\,km\,s^{-1}}$, D_L is the luminosity distance, and ν_obs is the observed frequency.

In Figure 2, we show a zoom-in on the *HST* image of the BCG and its surroundings (Webb et al. 2015a), with the LMT pointing position indicated. The LMT beam at 3 mm (100 GHz) is ~ 25 arcsec FWHM, which encompasses the ~ 100 kpc surrounding the BCG and all of the related substructure seen in Figure 2. Thus, the measured value for L'_CO should be taken as a lower limit since, if the peak of the emission is actually off-axis, centered on one of the clumps in the tidal tail for example, the beam response function will result in an under-estimate of the emission. We note, however, that there is only one *Spitzer Space Telescope* MIPS source within the beam, and it is within 2 arcsec of the pointing center. This source is detected at a significance of 10σ.

3.2. Inferred Gas Properties

The integrated source brightness temperature, determined in the previous section, can be used to estimate the total mass of molecular hydrogen (Solomon et al. 1992):

$$\frac{M_\mathrm{H2}}{M_\odot} = \frac{\alpha_\mathrm{CO}}{r_{J1}} \frac{L'_{(J-[J-1])}}{\mathrm{K\,km\,s^{-1}\,pc^2}},\quad (2)$$

where α_CO is the CO-to-H_2 conversion factor and r_{J1} provides a correction from the flux of the higher-order J transitions to that of CO(1–0). Here, we adopt an r_{21} value of 0.85 (Carilli & Walter 2013) and $\alpha_\mathrm{CO} = 0.8\ M_\odot\ (\mathrm{K\,km\,s^{-1}\ pc^2})^{-1}$; this is appropriate for ultraluminous infrared galaxies (ULIRGs) and provides a conservative estimate on the total gas mass. We find
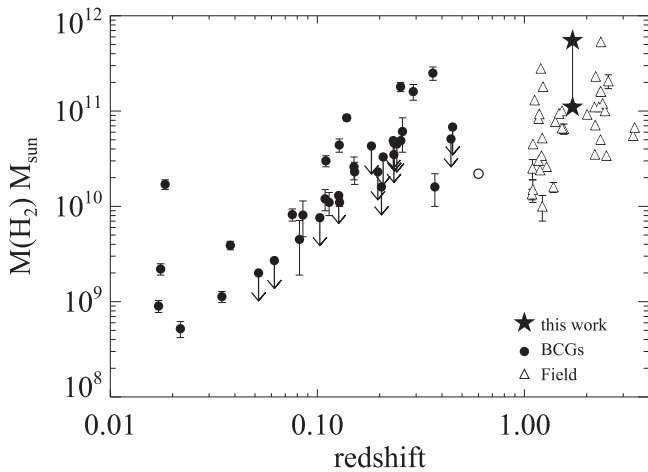
Figure 3. Compilation of molecular gas masses, shown as a function of redshift. Note that as this is not a complete nor homogeneously selected sample, an evolutionary trend should not be drawn from these points. We show the values simply to place the molecular gas mass of this work in the context of other, similar measurements. SpARCS1049 is denoted by the solid star. Solid circles correspond to BCGs from Edge (2001), McNamara et al. (2014), Russell et al. (2014), and Vantyghem et al. (2016), with the open circle showing the location of the Phoenix BCG (McDonald et al. 2013). Open triangles indicate star-forming field galaxies from Genzel et al. (2010) and Decarli et al. (2016). These studies have each chosen the α_{CO} conversion factor deemed most appropriate for their respective systems, ranging from 0.8 to $4.0\,M_{\odot}$ (K km s^{-1} pc^2)$^{-1}$; in the text, we use $\alpha_{CO} = 0.8\,M_{\odot}$ (K km s^{-1} pc^2)$^{-1}$, but on this plot we illustrate, with two points, the full range in mass that results from the range in α_{CO}.

a molecular gas mass of $1.1 \pm 0.1 \times 10^{11}\,M_{\odot}$. We note, however, that, as reviewed by Carilli & Walter (2013) and Bolatto et al. (2013), the CO-to-H2 conversion is subject to some uncertainty, especially for star-forming systems and can be as high as $\alpha_{CO} \sim 4\,M_{\odot}$ (K km s^{-1} pc^2)$^{-1}$ for main-sequence galaxies (Decarli et al. 2016; Daddi et al. 2010a).

4. Discussion

The precise line fitting provides us with a very accurate redshift for the CO gas of 1.7091 ± 0.0004. This is in excellent agreement with the systemic redshift of the galaxy cluster (Webb et al. 2015a) of $z = 1.709 \pm 0.001$, estimated from an average of optical redshifts of 27 confirmed cluster members (Webb et al. 2015a). This suggests that the CO emission is indeed coming from the center of the cluster potential, spatially near the BCG, and is not a projection along the line of sight from a galaxy on the outskirts of the cluster.

Thus, these results indicate that a vast reservoir, $1.1 \pm 0.1 \times 10^{11}\,M_{\odot}$, of molecular gas has been deposited into the center of this galaxy cluster and has formed the fuel source for a phase of rapid star formation. To place this measurement in context, we show in Figure 3 a compilation of molecular gas masses for comparable systems. We include the massive star-forming galaxies at $z > 1$ from Genzel et al. (2010) and Decarli et al. (2016) as well as lower-redshift ($z < 0.6$) BCGs (Edge 2001; McDonald et al. 2013; McNamara et al. 2014; Russell et al. 2014; Vantyghem et al. 2016). SpARCS1049 lies at the average of the mass distribution for CO-detected systems.

In Webb et al. (2015a), before the CO detection presented here, we speculated that the gas feeding the star formation might have been transported from the outskirts of the cluster via a single gas-rich massive galaxy, due to the merger-like optical morphology of the system. At low redshift such an event is generally thought to be difficult to achieve due to the removal of the interstellar medium (ISM) of infalling galaxies by the intracluster medium (ICM). At high redshift, however, galaxies not only start their descent into the galaxy cluster potential with higher fractions of molecular gas, clusters themselves are younger and may have ICMs that are less effective at ISM removal than at low redshift. While the major-merger picture is in line with other studies (McDonald et al. 2016), these data now raise several questions.

The emission is well fit by a single Gaussian and shows no sign of multiple velocity peaks. This is perhaps unexpected given the multiple spatial components and merger-like morphology seen in the rest-frame optical (Figure 2) and is also unlike many other CO-detected systems at high redshift. The sample of Greve et al. (2005), for example, presents several cases (30%–50% of the sample) of dual-peaked CO spectra with velocity offsets of several hundreds km s^{-1}, which they conclude are produced through major mergers. Similar dynamic structure is seen in the famous local Antennae galaxies (Gao et al. 2001; Schulz et al. 2007). The lack of such a signature in our data raises the possibility, but is not unambiguous evidence, that the molecular gas, and thus the star formation, is not distributed over the same multiple objects as the optical/UV emission. Rather, it may be concentrated in a single dynamically distinct region.

We posit two possible scenarios in which a gas-rich merger is not required to produce the large amount of star formation we see. (1) The gas deposit may be the result of the stripping of many galaxies within the cluster center. In this case, it may be that the multiple stellar clumps have also come from several objects. Such a process would allow for a large build-up of gas thath would have a velocity dispersion that traces the overall velocity dispersion of the cluster. The velocity dispersion of the cluster is poorly constrained (430^{+80}_{-100} km s^{-1}), but given the existing velocities and its mass of $\sim 4 \times 10^{14}\,M_{\odot}$ (Webb et al. 2015a), it is roughly a factor of two larger than the velocity dispersion of the gas (Figure 1; FWHM ~ 560 km s^{-1} or $\sigma \sim 250$ km s^{-1}). This is weak evidence against the idea that the gas has been stripped from many cluster members. (2) The gas could flow to the center of the cluster through a large-scale cooling flow, as we see in many lower-redshift clusters (such as Phoenix; McDonald et al. 2013). The complex optical morphology may indicate that cooling has been been triggered through the disruption of centralized heating processes via a collision between an infalling galaxy and the BCG (M. Voit 2017, personal communication).

Using our ancillary data we can attempt some interesting comparisons to measurements at other wavelengths in the hope they may shed light on the origin of the gas. Perhaps the simplest is the relation between the molecular gas luminosity (L'_{CO}) and the total infrared luminosity (L_{IR}), since it is likely these emissions are indeed spatially co-located. Several sources of infrared imaging are available for this cluster: *Herschel* Space Observatory, *Spitzer Space Telescope*, and the James Clerk Maxwell Telescope. We reiterate that in the highest-resolution infrared imaging available (*Spitzer Space Telescope* MIPS) there is only one infrared source within the 25 arcsec LMT beam, and therefore it is unlikely that the CO emission is coming from multiple sources separated by more than a few arcseconds. The infrared luminosity was measured in Webb et al. (2015a) by fitting a template spectral energy distribution
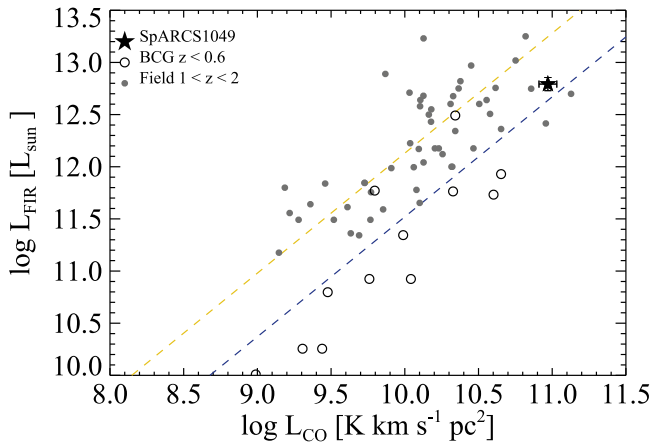
Figure 4. Relation between L_{CO} and L_{FIR}. Included are systems between $1 < z < 2$ with published CO measurements (gray points; Carilli & Walter 2013 and references therein) and lower-redshift ($z < 0.6$) IR-bright BCGs (Edge 2001; O'Dea et al. 2008; Rawle et al. 2012). We take the lowest CO transition available and correct it, following Carilli & Walter (2013), to CO (1–0). The two dotted lines correspond to the best-fit relations for main-sequence galaxies (blue) and starburst galaxies (yellow) of Daddi et al. (2010b) and Genzel et al. (2010). The solid black star indicates the values measured for the SpARCS1049 BCG system.

Figure 5. Ratio of molecular gas mass to stellar mass ($M_{H2}/M_\star$) for several star-forming field galaxies from the literature (gray points; Leroy et al. 2008; Daddi et al. 2010a; Genzel et al. 2010; Riechers et al. 2010; Tacconi et al. 2010; Geach et al. 2011; Magnelli et al. 2012; Silverman et al. 2015; Decarli et al. 2016; Papovich et al. 2016). The solid line corresponds to the relation from Geach et al. (2011). As in Figure 3, different α_{CO} values have been employed, nor have we attempted to normalize the stellar mass measurements to the same IMF (although the bulk of the studies adopt a Chabrier IMF). Because of this, scatter at the level of a factor of two is expected in the $M_{H2}/M_\star$ measurements.

to the $24/250/350/450/500/850\,\mu m$ flux measurements. In Figure 4, we show the position of the SpARCS1049 BCG system on the L'_{CO}–L_{IR} plane, compared to several other measurements of field galaxies at $z > 1$ and lower-redshift BCGS, drawn from the literature. We see that although SpARCS1049 is extreme in its properties, in that it is relatively IR- and CO-bright, it lies within the distribution of other infrared luminous galaxies at similar redshifts, inside and outside of clusters.

These measurements indicate that even with such a large reservoir of molecular gas, the gas consumption timescale of SpARCS1049+56 remains rapid, $\langle\tau_{gas}\rangle = M_{H2}/SFR \sim 0.1$ Gyr, because of the prodigious SFR. Although on the short end, this is within the normal range of local and high-redshift star-forming galaxies (Saintonge et al. 2011). Concerning the origin of the gas, however, the comparison has very little diagnostic power. The literature sample comprises a heterogeneous mixture of QSOs, HzRGs, SMGs, 24 μm-selected, BzK, ERO, and BMBX galaxies as well as cooling-flow-fed BCGS. Thus, despite the fact that these galaxies likely have different gas accretion mechanisms (mergers, cold-flows, cluster cooling flows), they exhibit similar L'_{CO}–L_{IR} properties.

The molecular mass to stellar mass ratio ($M_{H2}/M_\star$) is shown in Figure 5. This is a difficult quantity to estimate because we do not know from which stellar mass component the CO originates. We adopt the stellar mass of the BCG (Webb et al. 2015a) and see once again that this value of $M_{H2}/M_\star \sim 0.4$ is in good agreement with that of other high-redshift ULIRGs. We do not compare to the values of lower-redshift BCGs in this case as the BCGs of Edge (2001) do not have published stellar masses. This agreement with field systems indicates that if the source of the gas was a single accreted galaxy, it must have had a mass within a factor of ~ 5 of the BCG mass; otherwise, $M_{H2}/M_\star$ would be too high, in comparison to other similar systems. Alternatively, this ratio could be explained by the accretion of several lower-mass galaxies, each with a $M_{H2}/M_\star \sim 0.4$.
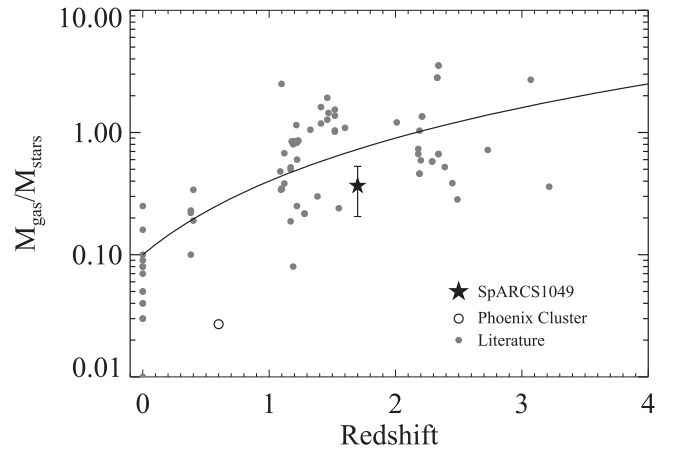
Understanding the role of the three possible gas deposition processes—major merger, multiple galaxies, cooling flow— will clearly require additional observations, such as X-ray imaging or high-resolution integral field spectroscopy. More-over, the synthesis of these results with data at other wavelengths is not straightforward due to the confused morphology of the system and the large beam size of the facility used in this study, since it is not possible to tell from these data physically where the CO emission originates (recall Figure 2). Because of this, higher-resolution CO observations are imperative. Finally, although SpARCS1049+56 has been drawn from a larger sample of BCGs, we do not yet know if it is representative, and thus more CO observations of high-redshift BCGs are warranted.

5. Conclusions

We report the 10.7σ detection of molecular gas, via CO(2–1) observations with the LMT, in the center of the $z = 1.7$ galaxy cluster, SpARCS1049+56. This is the first detection of molecular gas coincident with a BCG above $z > 1$. We draw several conclusions:

1. The high-precision redshift of the CO(2–1) line of $z = 1.7091 \pm 0.0004$ indicates that the molecular gas is located at the center of the gravitational potential of the cluster. It is therefore unlikely that the CO emission is due to a cluster member seen along the line of sight to the BCG.

2. The CO (2–1) line is well fit by a single Gaussian and shows no evidence for multiple velocity peaks. Its broad width of FWHM $569 \pm 63\,km\,s^{-1}$ ($\sigma = 250\,km\,s^{-1}$) is nevertheless much narrower than the expected overall velocity dispersion of the cluster.

3. Although it lies on the upper end of the relation, the L'_{CO}–L_{IR} ratio of the system is in good agreement with that of other galaxies at similar redshifts ($1 < z < 2$). These galaxies include extreme systems such as the cooling-flow-fed

star-forming BCG of the Phoenix cluster and merging SMGs, to more "normal" BzK systems.

4. We infer a molecular gas mass of $M_{H2} = 1.1 \pm 0.4 \times 10^{11} M_{\odot}$. Employing the infrared-estimated SFR yields a gas depletion timescale of ~ 0.1 Gyr. Adopting the stellar mass of the BCG provides an $M_{H2}/M_{\star}$ value consistent with other high-redshift ULIRGs ($M_{H2}/M_{\star} \sim 0.4$).

5. Although we posit several gas deposition mechanisms, these data are not able to differentiate between them. We conclude that more data are required to establish if the immense gas reservoir at the center of this system has been fed by a cooling flow, a major galaxy–galaxy merger, or the stripping of gas from several galaxies.

References

Bolatto, A. D., Wolfire, M., & Leroy, A. K. 2013, ARA&A, 51, 207
Bonaventura, N. R., Webb, T. M. A., Muzzin, A., et al. 2017, MNRAS, 469, 1259
Carilli, C. L., & Walter, F. 2013, ARA&A, 51, 105
Cybulski, R., Yun, M. S., Erickson, N., et al. 2016, MNRAS, 459, 3287
Daddi, E., Bournaud, F., Walter, F., et al. 2010a, ApJ, 713, 686
Daddi, E., Elbaz, D., Walter, F., et al. 2010b, ApJL, 714, L118
De Lucia, G., & Blaizot, J. 2007, MNRAS, 375, 2
Decarli, R., Walter, F., Aravena, M., et al. 2016, ApJ, 833, 70
Edge, A. C. 2001, MNRAS, 328, 762
Gao, Y., Lo, K. Y., Lee, S.-W., & Lee, T.-H. 2001, ApJ, 548, 172
Geach, J. E., Smail, I., Moran, S. M., et al. 2011, ApJL, 730, L19
Genzel, R., Tacconi, L. J., Gracia-Carpio, J., et al. 2010, MNRAS, 407, 2091
Greve, T. R., Bertoldi, F., Smail, I., et al. 2005, MNRAS, 359, 1165
Hughes, D. H., Jáuregui Correa, J.-C., Schloerb, F. P., et al. 2010, Proc. SPIE, 7733, 773312
Leroy, A. K., Walter, F., Brinks, E., et al. 2008, AJ, 136, 2782
Lidman, C., Suherli, J., Muzzin, A., et al. 2012, MNRAS, 427, 550
Magnelli, B., Saintonge, A., Lutz, D., et al. 2012, A&A, 548, A22
McDonald, M., Benson, B., Veilleux, S., Bautz, M. W., & Reichardt, C. L. 2013, ApJL, 765, L37
McDonald, M., Stalder, B., Bayliss, M., et al. 2016, ApJ, 817, 86
McDonald, M., Swinbank, M., Edge, A. C., et al. 2014, ApJ, 784, 18
McNamara, B. R., Russell, H. R., Nulsen, P. E. J., et al. 2014, ApJ, 785, 44
Muzzin, A., Wilson, G., Yee, H. K. C., et al. 2009, ApJ, 698, 1934
O'Dea, C. P., Baum, S. A., Privon, G., et al. 2008, ApJ, 681, 1035
Papovich, C., Labbé, I., Glazebrook, K., et al. 2016, NatAs, 1, 0003
Rawle, T. D., Edge, A. C., Egami, E., et al. 2012, ApJ, 747, 29
Riechers, D. A., Carilli, C. L., Walter, F., & Momjian, E. 2010, ApJL, 724, L153
Russell, H. R., McNamara, B. R., Edge, A. C., et al. 2014, ApJ, 784, 78
Russell, H. R., McNamara, B. R., Fabian, A. C., et al. 2016, MNRAS, 458, 3134
Saintonge, A., Kauffmann, G., Wang, J., et al. 2011, MNRAS, 415, 61
Schulz, A., Henkel, C., Muders, D., et al. 2007, A&A, 466, 467
Silverman, J. D., Daddi, E., Rodighiero, G., et al. 2015, ApJL, 812, L23
Solomon, P. M., Downes, D., & Radford, S. J. E. 1992, ApJL, 387, L55
Tacconi, L. J., Genzel, R., Neri, R., et al. 2010, Natur, 463, 781
Vantyghem, A. N., McNamara, B. R., Russell, H. R., et al. 2016, ApJ, 832, 148
Webb, T., Noble, A., DeGroot, A., et al. 2015a, ApJ, 809, 173
Webb, T. M. A., Muzzin, A., Noble, A., et al. 2015b, ApJ, 814, 96
Wilson, G., Muzzin, A., Yee, H. K. C., et al. 2009, ApJ, 698, 1943
Zhang, Y., Miller, C., McKay, T., et al. 2016, ApJ, 816, 98